Particle-in-Cell Code Simulations of the Interaction of Gaussian Ultrashort Laser Pulses with Targets of Varying Initial Scale Lengths

Introduction

Since the advent of ultrashort laser pulses[1] there has been interest in the interaction of such pulses with solid targets. Several new modes of laser-plasma interaction at high intensities ($I\lambda^2 > 10^{16}$ W/cm^2 μm^2) have been identified, the most important being "vacuum heating,"[2] which dominates over resonance absorption when scale lengths are very short. These new absorption mechanisms, as well as nonlinear resonance absorption (wave breaking), are usually studied with a PIC (particle-in-cell) code. In one series of published results from PIC simulations, the interaction of p-polarized light with a plasma over a wide range of irradiances and scale lengths is described.[3] The range covered in these simulations included the transition from resonance absorption to vacuum heating. The simulations were carried out for a constant pulse, and few details were provided on the behavior of the fields and of the plasma. Other published results of PIC simulations[4] have concentrated on the effect of the radiation pressure on the motion of the ions at intensities in excess of 10^{18} W/cm^2 μm^2. Above this intensity the interaction enters another regime in which relativistic effects become important. We will not deal with the relativistic regime in this article. Incidentally, Vlasov codes have also recently been developed to study these nonlinear absorption mechanisms.[5]

Here, we present simulations in which a 100-fs Gaussian pulse interacts with preformed plasmas of varying scale lengths. These calculations simulate many of the actual experimental conditions in which laser pulses are preceded by either a long ASE pulse or a pedestal due to imperfect pulse expansion and recompression in chirp-pulsed amplification schemes. These simulations, carried out at an irradiance of 10^{16} W/cm^2 μm^2, near the irradiances reached in many experiments, include ion motion. A set of simulations was carried out with electron-ion collisions included. We find that observables like the absorption fraction, the fast-electron and fast-ion energy, and the production of harmonics depend strongly on the scale length of the initial profile.

The calculations were carried out with the 1 1/2-D relativistic PIC code *EUTERPE*.[6] Electron scattering due to collisions with the ions is included using a Monte Carlo rotator at the end of each time step.[7] To treat p-polarized oblique incidence, simulations are done by transforming to a reference frame moving in the transverse direction with velocity $v_d = c \sin\theta$, where θ is the angle of incidence.[3] This method suffers from two limitations: First, it does not model rippling of the critical surface, which becomes significant above 10^{18} W/cm^2 μm^2 and leads to a more complex angular distribution of the incident laser light. Second, at large angles, the maximum density, which transforms as $n_e/n_c = \gamma^{-3}(n_e/n_c)'$, where

$$\gamma = \left[1 - \left(\frac{v_d}{c}\right)^2\right]^{-1/2} = \sec\theta,$$

becomes very large, which forces the time step to be very small and the number of particles to be large in order to obtain reasonable results. Most of the runs were done with 50,000 particles and with a mesh size of 500–1000 grid points. The absorption fraction, defined as the internal energy in the plasma divided by the cumulative input energy, is calculated in two ways: In the first way, the internal energy in the plasma is obtained as the sum of the kinetic energy over all the particles minus the initial internal energy of the plasma. In the second way, the internal energy is calculated by subtracting the electromagnetic energy in the box from the time-integrated Poynting vector at the left (input) boundary. Ideally, these two methods should yield the same absorption fraction.

Transition from Resonance Absorption to Vacuum Heating

In vacuum heating,[2] the longitudinal electric field does not penetrate into the plasma because of the steep density gradient but reaches its maximum value in the vacuum near the plasma

boundary. When electrons penetrate into the vacuum with the right timing, they are accelerated outward by the large longitudinal electric field. They are then turned around by the oscillating field and the electrostatic potential and penetrate into the solid with velocity $v \approx v_{osc}$ where they deposit their energy. Vacuum heating becomes the dominant absorption mechanism when the oscillatory orbit of the electrons in the laser field becomes large compared to the scale length. This can occur for either very steep density gradient or very large laser intensity.

We will discuss the transition from resonance absorption to vacuum heating for the nonrelativistic intensity regime, $I\lambda^2 < 10^{18}$ W/cm^2 μm^2. We are especially interested in finding "observables," experimental and numerical, that lead to the definition of the regime. Experimental observables include the absorption fraction, the fast electron spectrum (deduced from hard x rays, K_α emission, and electron spectrometry), and the harmonic emission. Numerical observables include the experimental observables, the electron phase space, the electron trajectories, and the longitudinal electric field profile. Velocities are normalized to the velocity of light, positions to c/ω_0, and time to ω_0^{-1}, where ω_0 is the laser frequency.

The difference between resonance absorption and vacuum heating can be readily seen by plotting the electron trajectories (orbits) for two extreme scale lengths: $L/\lambda = 1$ and $L/\lambda = 0.001$, where λ is the laser wavelength. In Fig. 58.15(a), in which are plotted the trajectories of selected electrons (every 1000th) near the critical surface for a constant irradiance of 5×10^{16} W/cm^2 μm^2, an incident angle of 30°, and $L/\lambda = 1$, we observe the growth of the electron plasma wave until wave breaking starts at about 60 ω_0^{-1}. Wave breaking tends to occur in a random fashion in the resonance region when electron orbits cross. The electron trajectories for vacuum heating, shown in Fig. 58.15(b), show a very different behavior. In this case the conditions are a constant irradiance of 10^{18} W/cm^2 μm^2, an incident angle of 30°, and $L/\lambda = 0.001$. Starting with the first period of the laser, and for each successive period ($T = 2\pi$), electrons are pulled out into the vacuum and returned to the solid with velocities near v_{osc}. Interesting structures can also be observed: the successive long and short orbits into the vacuum every two laser periods and the smaller orbits with a "period" of one-half a laser period.

The difference in the longitudinal electric field profile for the two cases is shown in Fig. 58.16 along with the electron density profile. The electric field shown here, and in all subsequent graphs, is the oscillating field averaged over a period of the laser field normalized to the incident longitudinal electric field. In the resonance absorption case [Fig. 58.16(a)] the resonant field at the critical surface is large compared to the incident field and creates a "hole" in the density profile due to the ponderomotive force. In the vacuum heating case,

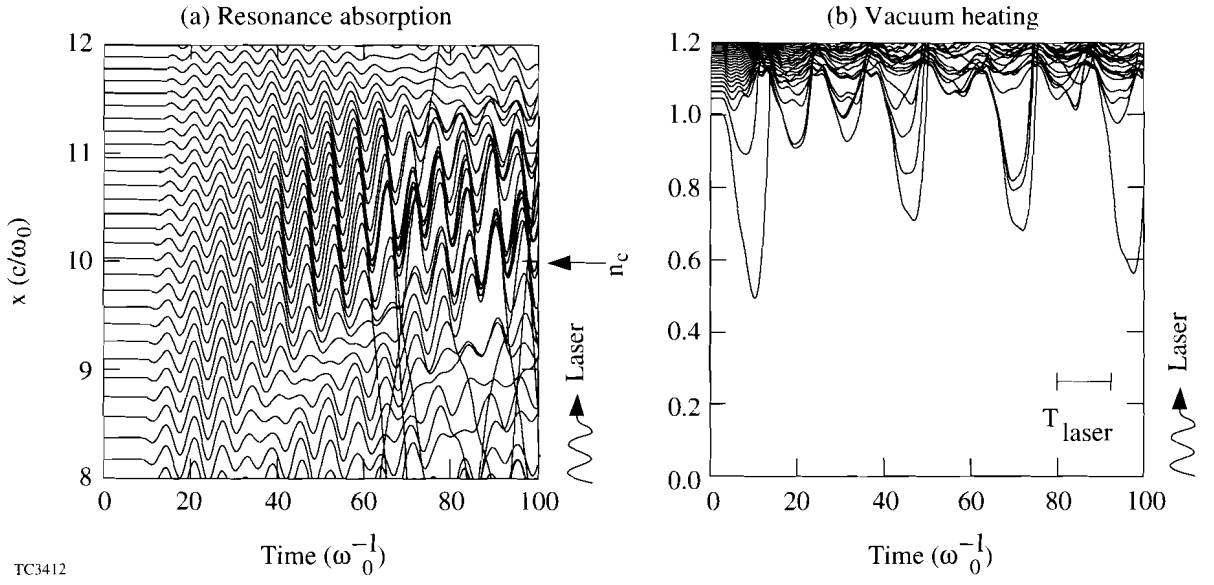

Figure 58.15
Electron trajectories for the two regimes: (a) resonance absorption; (b) vacuum heating. In both cases the laser is incident from the bottom. Only a sample of all the electrons is shown. Conditions are (a) $I\lambda^2 = 10^{16}$ W/cm^2 μm^2 and p-polarized light incident at 30°, $L/\lambda = 1.0$ linear, cold plasma without collisions, and stationary ions; (b) $I\lambda^2 = 10^{18}$ W/cm^2 μm^2 and p-polarized light incident at 30°, $L/\lambda = 0.001$ linear, cold plasma without collisions, and stationary ions.

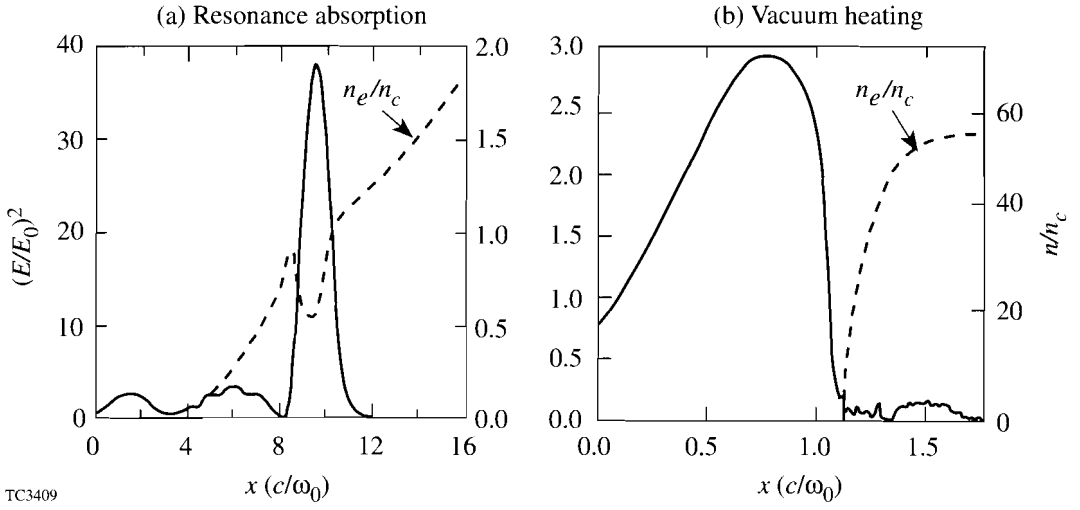

Figure 58.16
Period-averaged oscillating longitudinal electric field and electron density profile for the two cases in Fig. 58.15. The electric field is normalized to the incident longitudinal field.

the field does not penetrate into the plasma and displays the swelling expected near the surface of a conductor. The peak value of the field in the vacuum heating case is much lower than that in the resonance absorption case. As will be discussed below, this leads to much lower hot-electron energies for the same irradiance.

The transition from one regime to the other is complex, yet it is necessary to understand the changes that are occurring during this transition because many experiments are carried out under these conditions. The most straightforward way to study this transition is to vary the ion density profile, holding the irradiance fixed. In this way we avoid the added complexity that would arise from changes in such quantities as the absorption fraction and the electron maximum energy due to changes in the irradiance.

Interaction with Gaussian Pulses

Most, if not all, PIC simulations are carried out with a temporal irradiance characterized by a rising portion followed by a constant intensity up to some time limited by either computer time, by "numerical heating" due to the statistical nature of the problem, or by numerical instabilities in the code. These irradiation conditions approximate reasonably well those at the peak of pulses with pulse duration larger than tens of picoseconds; this may not be the case in ultrashort pulse laser interactions. With the advent of lasers with pulse duration of about 100 fs, it is now possible with present day computing power to simulate the interaction of an entire pulse with a plasma. Of course, PIC codes cannot simulate realistically high-density plasma in which electrons are described by Thomas-Fermi statistics and ions by short-range interaction. Atomic physics processes such as ionization and radiation are not included in PIC codes, although some effort is being made to include ionization.[7]

In this section we present the results of the study of the interaction of a 100-fs Gaussian pulse (full-width at half-maximum) with plasmas of varying initial electron and ion density scale lengths. The initial scale length is varied in order to simulate many present day experiments in which a prepulse creates a plasma in front of the solid surface before the arrival of the main pulse. Simulations with a Gaussian pulse can model more realistically than constant pulses the production of fast ions and the effect of the temporal variation of the irradiance on the absorption fraction, on the production of fast electrons and ions and of harmonics, and on the distortion of the density profiles due to the ponderomotive force. The simulations include ion motion and, in some cases, electron-ion collisions. In the collisionless case the ions have a charge of unity and a mass of 3600 m_e. In the collisional case, the simulations are specialized to fully ionized aluminum ($Z = 13$) and a laser wavelength of 620 nm [the wavelength of a CPM (chirped pulse modulated) dye laser]. The irradiance is started and stopped at 1% of the peak power, taken to be 10^{16} W/cm^2 μm^2. The simulations were carried out at a 30° angle of incidence and included 50,000 particles.

Four linear density profiles were used: $L/\lambda = 0.001$, 0.01, 0.1, 1.0. The following experimental diagnostics are displayed

for these four cases: the energy spectrum of the electrons that entered the solid (those reaching the high-density boundary), the energy spectrum of all the ions at the end of the pulse, and the cumulative absorption fraction as a function of time. The effect of the initial density profile on the electric field near or in the plasma and on the ion density profile at the end of the pulse will also be discussed.

We first discuss changes in the longitudinal electric field profile due to variations in the initial scale length, as displayed in Fig. 58.17. At the two extremes, $L/\lambda = 0.001$ and $L/\lambda = 1.0$, the electric field shows the behavior expected from vacuum heating and resonant absorption respectively. As the scale length is decreased from $L/\lambda = 1.0$, we observe the gradual change from the the single resonant peak to the wave swelling outside the steep plasma profile. Conditions at $L/\lambda = 0.1$ are complex: the resonant field is split and a resonance at $2\ n_c$ can be observed. At that scale length the resonant peak occurs near the edge of the plasma: the width of the resonant region is equal to or larger than the scale length and the orbits of the thermal electrons in that region can extend into the vacuum. As the gradient steepens to $L/\lambda = 0.01$, some field swelling in the vacuum interfaces can now be observed along with a resonance peak at the edge of the plasma and small multi-resonances in the overdense plasma. At the steepest gradient the field is confined to the vacuum and all resonances have disappeared.

The effect of the ponderomotive force due to the electromagnetic field on the ion density profile is shown in Fig. 58.18 at a time near the end of the pulse. The dashed line indicates the initial density profile. In the shortest scale length case, $L/\lambda = 0.001$, the pressure from the reflected laser beam is not large enough to move back the density profile during the pulse duration. Ions below the critical surface have expanded into the vacuum due to two effects: the pressure of the heated thermal electrons that have expanded into the vacuum and the electrostatic potential from electrons pulled into the vacuum by the vacuum heating absorption process. At such a short scale length the density gradient at the critical surface is not steepened, but lengthened due to the expansion. The medium-scale-length cases, $L/\lambda = 0.01$ and 0.1, show a slight deformation of the ion density profile. This effect is caused by the ponderomotive pressure of the resonant field situated at the edge of the plasma, not by the pressure of the reflected

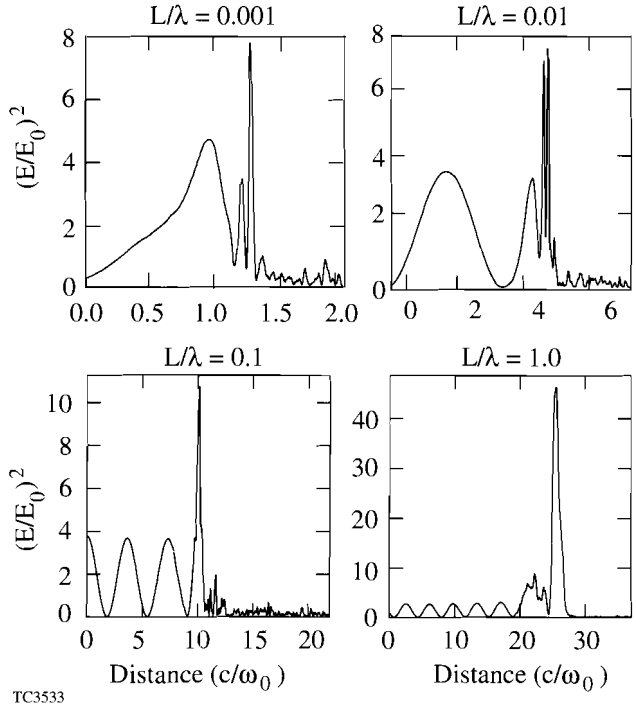

Figure 58.17
Period-averaged oscillating longitudinal electric field in the transition from resonance absorption to vacuum heating at the peak of the Gaussian pulse ($400\ \omega_0^{-1}$). Laser conditions are $I\lambda^2 = 10^{16}$ W/cm^2 μm^2 and p-polarized light incident at 30°; the initial density profiles are linear, and collisions are not included.

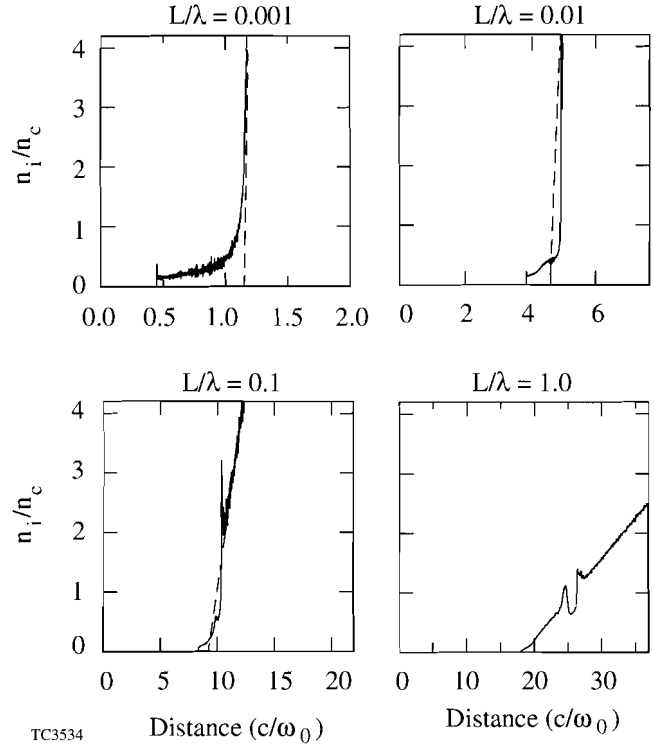

Figure 58.18
Ion density profile at the end of the pulse for the conditions in Fig. 58.17. The dashed curve is the initial density profile.

light. At the peak of the pulse the profile steepening is slight and should not affect the resonant absorption process. At the end of the pulse the profile for the case $L/\lambda = 0.1$ was steepened to $L/\lambda = 0.025$. Profile modification is more evident in the long-scale-length case because the resonant field is larger than at shorter scale lengths. At the peak of the pulse a small plateau is created, and the local scale length at the critical surface is about 0.5 λ. By the end of the pulse a hole about 0.5 n_c deep has been dug into the ion density profile by the resonant electric field.

One of observables strongly affected by variations in the scale length is the harmonic emission, plotted in Fig. 58.19. For the case $L/\lambda = 1$ we observe the harmonic emission expected from resonance absorption: an exponentially decreasing series of harmonics. For $L/\lambda = 0.1$, the harmonic series is very noisy and is cut off above $n = 2$. The case $L/\lambda = 0.01$ is very interesting in that the emission occurs at half-harmonics: 3/2 and 5/2; we have found no explanation for this behavior. At the steepest gradient, very weak harmonics are observed at $n = 3$ and 4, but none at $n = 2$. The low harmonic level is probably due to the low absorption efficiency of the vacuum heating mechanism at this intensity. At higher intensities the entire range of harmonics can be observed.

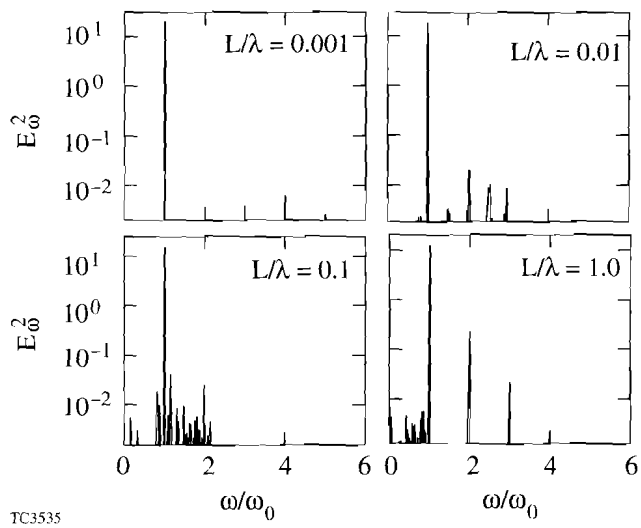

Figure 58.19
Power spectrum of the reflected light for the conditions in Fig. 58.17. Note the half-harmonics produced in the case $L/\lambda = 0.01$.

The spectra of the electrons that have left the computational box at the high-density end for the four cases are shown in Fig. 58.20. These are electrons that create observable bremsstrahlung hard x rays and K_α emission from the solid target. The maximum energy of the electrons decreases with scale length, in agreement with the decreasing peak values of the electric field observed in Fig. 58.17. It is not straightforward to obtain a temperature from the spectra because the electron distribution is not Maxwellian, especially for the short-scale-length cases. One reason is that vacuum heating tends to produce beams of electrons rather than a distribution; the other reason is that the spectra are cumulative over a range of intensity, therefore over a range of temperatures. For $L/\lambda = 0.1$ and $L/\lambda = 1.0$, the distributions are nearly Maxwellian with temperatures of 22 keV and 35 keV respectively. For $L/\lambda = 0.001$ and $L/\lambda = 0.01$ the slopes of the main body of the distribution yield 6 keV and 10 keV, respectively.

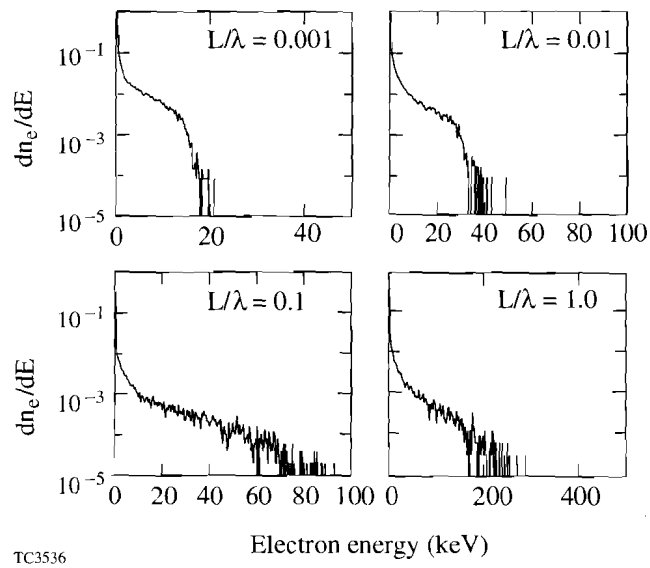

Figure 58.20
Cumulative distribution of the electrons entering the solid (leaving at the right-hand-side boundary) for the conditions in Fig. 58.17.

The ions spectra for the four cases, another experimental diagnostic, are shown in Fig. 58.21. The spectra contain the main body of the ion distribution at low energy and the distribution of the fast ions accelerated by the hot electrons. From $L/\lambda = 0.001$ to $L/\lambda = 0.01$, as expected the peak ion energy increases with scale length as did the hot-electron distribution. The increase is small between $L/\lambda = 0.01$ and $L/\lambda = 0.1$, and the peak energy is actually lower for $L/\lambda = 1$ than for $L/\lambda = 0.1$, despite the fact that the fast-electron energy increases sharply in that range of scale length. Two effects may be responsible for the scaling of the fastest ion energy: not enough time to accelerate the ions to their maximum velocity because of the short pulse duration; the

accelerating electrostatic potential, given roughly by T_h/L, where T_h is the hot-electron temperature, is lower in the long-scale-length cases.

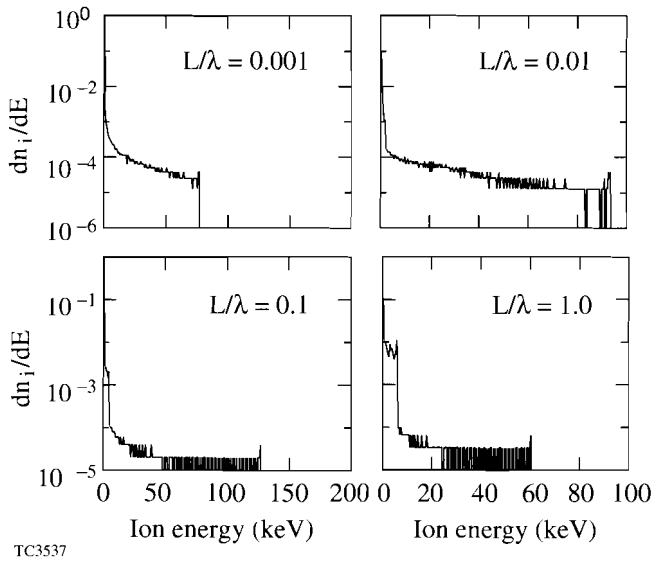

Figure 58.21
Total ion spectrum at the end of the pulse for the cases in Fig. 58.17. The energetic ions are the fast ions accelerated into the vacuum.

The cumulative absorption fraction as a function of time is plotted in Fig. 58.22 for the four cases. The peak of the pulse is at 400 ω_0^{-1}. In these graphs, the absorption fraction is defined as the time-integrated Poynting vector at the vacuum boundary minus the electromagnetic energy in the computing box, divided by the time-integrated input laser energy at the vacuum boundary. The "hash" in the line is due to the time-varying value of the electromagnetic energy in the box. The final absorption fraction is low at the short scale lengths (about 10%) and increases with scale length as the resonance absorption regime becomes dominant. Adding collisions ($Z = 13$) has little effect on these results: the absorption fraction is slightly larger early in the pulse but is slightly lower near the peak of the pulse because collisions decrease slightly the resonant field. At this intensity vacuum heating is a very inefficient absorption process.

The results of the simulations are summarized in Fig. 58.23 where the absorption fraction and the maximum electron and ion energy are plotted as a function of the scale length. The absorption remains very low for $L/\lambda < 0.01$ and increases for increasing scale length to the large values associated with resonance absorption. The electron peak energy scales roughly as $(L/\lambda)^{0.4}$, except through the vacuum heating range where it would be expected to depend only on the laser intensity through v_{osc}. These results, and the behavior of the longitudinal electric field, point to the existence of three regions as discussed in Ref. 3: the vacuum heating region below $L/\lambda = 0.01$; a region in which the oscillatory orbit of the electrons is about the distance between the critical surface and the vacuum/plasma interface; and a resonance absorption region above $L/\lambda = 0.03$, where the resonance occurs inside the plasma and the oscillating electrons never reach the vacuum. The second region is very complex. The resonance structure of the electric field splits for some values of L/λ, while harmonic resonances appear in the overdense plasma. A detailed study of the electron orbits shows that the electrons near the plasma/vacuum interface can be accelerated into the vacuum without undergoing wave breaking, while electrons slightly deeper in the plasma, but still in the resonance region, are accelerated by wave breaking. The different regimes can be seen as plateaus in the absorption fraction separated by transition regions. Similar results, but slightly shifted to higher scale lengths, were obtained for an irradiance of 10^{17} W/cm^2 μm^2: The transition to vacuum heating occurs now for $L/\lambda \approx 0.03$ as compared to $L/\lambda \approx 0.01$ for the lower irradiance case.

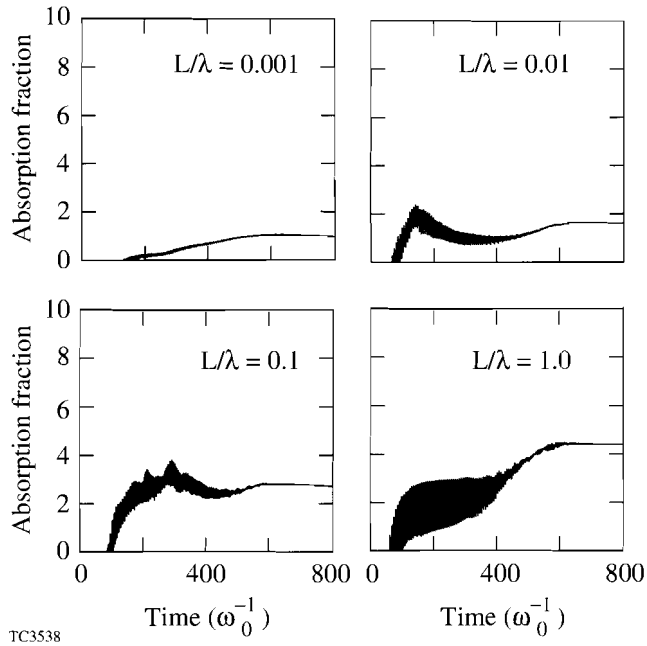

Figure 58.22
Cumulative absorption fractions for the conditions in Fig. 58.17. The "hash" in the line is due to the time-varying value of the electromagnetic energy in the box.

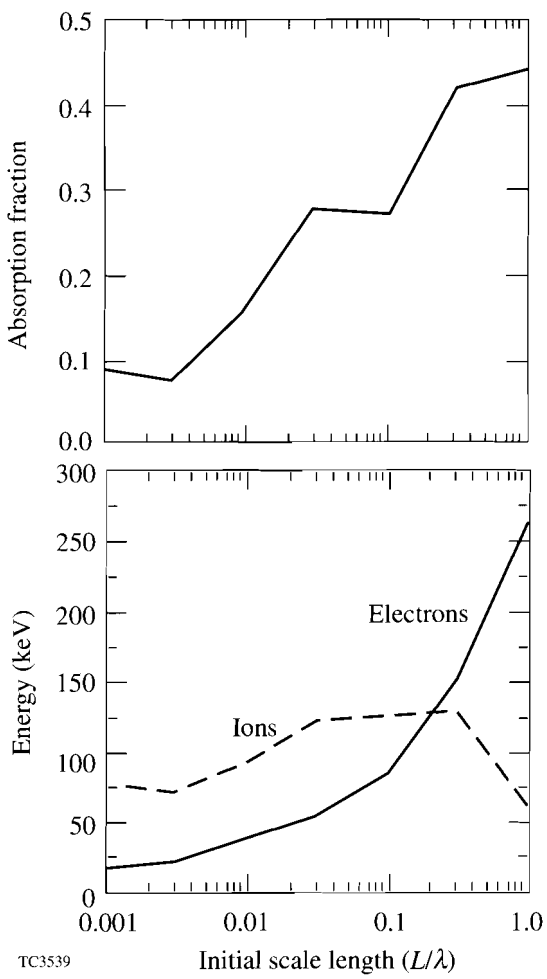

Figure 58.23
Summary of the results from the simulations of the transition from vacuum heating to resonant absorption for conditions in Fig. 58.17.

Conclusions

The transition from the resonance absorption regime to the vacuum heating regime in short-pulse laser-plasma interaction has been studied using the 1 1/2-D PIC code *EUTERPE*. Laser conditions were a 100-fs Gaussian pulse with $I\lambda^2 = 10^{16}$ W/cm^2 μm^2 and p-polarized light incident at 30°. The transition was observed by varying the density scale length over the range $L/\lambda = 0.001$ to 1.0.

We observed that vacuum heating occurred for $L/\lambda < 0.01$. This is a very steep scale length that can be obtained only with very short pulses (about 100 fs) in the absence of any prepulse energy on the target. For $0.3 > L/\lambda > 0.01$ the resonant region remains at the edge of the plasma. In this transition regime the behavior of the resonant field becomes complex as the orbits of the resonant electron extend into the vacuum. For $L/\lambda > 0.3$, the resonance region moves into the plasma, and the "classic" resonance absorption regime is recovered. The peak resonant longitudinal electric field, the peak electron energy, and the absorption fraction increase with increasing scale length. Harmonic production above the second harmonic disappears in the transition regime. Adding collisions with $Z = 13$ has little effect on these results.

ACKNOWLEDGMENT

This work was supported by the Laboratoire pour l'Utilisation des Lasers Intenses and the Laboratoire de Physique des Milieux Ionisés, Ecole Polytechnique, Palaiseau, France and by the Centre d'Etude de Limeil-Valenton du Commissariat à l'Energie Atomique, Villeneuve-St-Georges, France. This work was also supported by the U.S. Department of Energy Office of Inertial Confinement Fusion under Cooperative Agreement No. DE-FC03-92SF19460, the University of Rochester, and the New York State Energy Research and Development Authority. The support of DOE does not constitute an endorsement by DOE of the views expressed in this article.

REFERENCES

1. P. Main and G. Mourou, Opt. Lett. **13**, 467 (1988).
2. F. Brunel, Phys. Rev. Lett. **59**, 52 (1987).
3. P. Gibbon and A. R. Bell, Phys. Rev. Lett. **68**, 1535 (1992).
4. For example, J. Denavit, Phys. Rev. Lett. **69**, 3052 (1992).
5. H. Rhul and P. Mulser, presented at the *23rd Annual Anomalous Absorption Conference*, Wintergreen, VA, 21–25 June 1993, paper 2O3.
6. G. Bonnaud and G. Reisse, Nucl. Fusion **26**, 633 (1986).
7. J. M. Wallace *et al.*, Phys. Fluids **3**, 2337 (1991).